A new approach for water crystallization in the kinetics-limited growth region

Antonio Criscione[1,2], Daniel Kintea[1,2], Ilia V. Roisman[1,2], Suad Jakirlić[1,2], Cameron Tropea[1,2]

[1]*Institute of Fluid Mechanics and Aerodynamics, Technical University of Darmstadt, Germany,*
[2]*Center of Smart Interfaces, Technical University of Darmstadt, Germany*

Keywords: supercooled water, dendritic growth, kinetic effects, morphological instability, array of needles, level set

Abstract

The crystallization mechanism of pure water in a supercooled state is not well understood so far. There are many open-ended questions about the basic physics of crystallization. A new computational model using an appropriate level set formulation for the numerical capturing of the interface between the supercooled and the solidified liquid is applied. Mathematically, the phenomenon of solidification is modeled by utilizing a moving boundary problem. Recent numerical results of dendritic growth (Criscione et al. 2012) exhibit excellent qualitative and quantitative agreement with the Marginal Stability Theory (Langer & Müller Krumbhaar 1978a, 1978b, 1978c) as well as with the available experiments (Furukawa & Shimada 1993, Ohsaka & Trinh 1998, Shibkov et al. 2001, 2003, 2005) in the heat-diffusion-dominated region. At higher supercoolings (in the so-called kinetics-limited region), an explicit deviation from experiments is observed. In the published literature the kinetic effects are indicated as a possible reason for this deviation, approximating the kinetic undercooling as a linear function of the interface velocity. Based on this assumption, a new approach for the calculation of the kinetic undercooling term is derived. This model results in an approximation for the kinetic coefficient which establishes a non-linear dependency between the kinetic undercooling and the velocity of the solid-liquid interface. Furthermore, investigations concerning the growth of needles in an array indicate that surrounding needle-like dendrites influence considerably the steady-state tip velocity of an isolated needle. This phenomenon depends directly on the spacing between the needles. In the present work an attempt is undertaken to explain a new approach for the physical description of the crystallization mechanism at higher supercooling.

I. Introduction

Water droplets which exist in liquid form at temperatures below 273,15 K (0°C) are defined as supercooled water droplets. They often occur in clouds which are located at altitudes which aircrafts usually have to pass during start and landing. The terminology often used regarding the in-flight airframe icing classifies them as Supercooled Large Droplets (SLD). SLD are defined in accordance with "The World Meteorological Organization" as those water droplets with a diameter larger than 50 microns. The large mass of a SLD will prevent the pressure wave travelling ahead of an airfoil from deflecting it. When this occurs, the droplet will impinge further back compared to a typical cloud-sized droplet, possibly beyond the protected area (leading edge area of the airfoil). This results in the formation of an ice layer on the rear part of the airfoil. At the time instant corresponding to the droplet impact, the crystallization of the water is triggered, causing any free nuclei in the supercooled liquid may be growing, often creating dendritic crystals. When water crystallizes, latent heat of fusion is released. If an SLD freezes, in fact only a small portion of the drop will freeze instantaneously, not more than enough to raise the temperature to the crystallization/melt temperature of 273.15 K. Further progressive freezing takes place as the droplet loses heat by evaporation and conduction. The phenomenon of in-flight airframe icing is recognized as a significant aviation hazard. It leads to increased aerodynamic drag and weight, associated with a reduction in lift and thrust. Icing is not only an aviation problem. Wind turbines are also hardly affected by icing. The problem with ice on an operating turbine is that it causes additional drive-train loads, excessing often the design loads. For this reason many turbines are shut down at icing onset; restarts are activated only after an inspection confirms that the ice retrieved. This is a cumbersome practice, especially in remote locations and at night, limiting drastically the economic profit of wind power plants.

Theoretically, the common approach to crystallization problems depends on the grade of the initial supercooling in the liquid. At low supercooling degrees, the freezing process can be considered as a Stefan problem corresponding to diffusion-driven growth (Alexiades & Solomon 1993). The solid-liquid interface is an active free boundary (moving boundary) from which the latent heat of freezing is released during the phase transformation. This heat is conducted away from the interface through both the liquid and the solid phase. The heat equation is solved in each phase separately. Both temperature fields, in the liquid and in the solid phase, are coupled through two boundary conditions at the moving

boundary. The first boundary condition is the constant melting/crystallization temperature at the interface. This temperature will be locally altered by an amount depending on the interfacial tension between the solid and liquid phases and the local curvature (Gibbs-Thomson effect). The second boundary condition is represented implicitly by the velocity of the moving boundary. It is derived from a heat balance at the interface (Stefan condition) and hence it depends on how fast the latent heat of solidification is removed from the interface. In the case of increasing supercooling, the literature reports that the so-called kinetic effects start to dominate the system. Thus, the slowest process of the freezing mechanism depends on how fast the liquid molecules can be brought in the proper position, orientation and conformation pertinent to the solid phase. The transition from heat-diffusion to kinetics-limited growth has been observed in experiments at a supercooling of approximately 10 K (Shibkov et al. 2005). The shape of the solid-liquid interface depends on various parameters such as the initial degree of supercooling, the surface tension and its anisotropy. In case that the initial supercooling of the liquid is low and the heat flux into the solid is high, usually planar solidification will occur. The latent heat of solidification released at the interface is mainly transferred into the solid phase. The more heat is conducted into the liquid the more unstable becomes the shape of the solid-liquid interface. At higher degrees of supercooling in the liquid phase the planar solidification front transforms to dendrite shaped surface with side-branching growth. Arrays of branchless dendrites (needle-like crystals) emerge at higher degrees of supercooling. Shibkov et al. (2001, 2003, 2005) investigated the free growth of an ice crystal in pure supercooled water. The experiments were performed on a horizontal 200 μm thick water film stretched over area of 30 mm^2. In order to seed an ice crystal in the supercooled water and hence to trigger the nucleation process they used a thin steel frosted rod. Various shapes of ice crystal patterns in the range between low (ΔT = 0.1 K) and high (ΔT = 14.5 K) supercooling have been observed (Figure 1). It becomes evident that, as mentioned before, the shape of the solidification front depends strongly on the initial degree of supercooling in the water film. Furthermore, the shape of the dendritic front is determined by the balance between surface energy criterion and the efficiency of the interface in removing heat. The study of the influence of disturbances at the interface, the so-called morphological instability anlysis, has been introduced by Mullins & Sekerka (1963a, 1963b).

Over the last decades, various computational approaches have been developed and applied to simulate crystallisation especially in metals. The existing computational models describing the solidification of pure water are not numerous. The direct solution of the time-dependent moving-boundary problem, which governs both the planar solidification and dendritic crystal growth, represents a great challenge. To date, the phase-field method has been usually used in simulations describing crystallisation phenomena to avoid the emerging difficulties in tracking a sharp boundary (Kobayashi 1993, Wheeler 1993, Do-Quang & Amberg 2008). In this work, a new computational model based on the level set technique (Osher & Sethian, 1988) is used (Criscione et al. 2012). It describes freezing mechanism under supercooled conditions relying on the physical and mathematical description of the two-phase moving-boundary problem. The relevant numerical algorithm is implemented into the open source software OpenFOAM®. In the next section an outline of the physics governing the freezing mechanism (moving-boundary problem) and its mathematical description is given. The level set algorithm used in this work is briefly introduced in section III. Furthermore, the transition from heat-diffusion dendritic growth to the kinetics-limited region is investigated in section IV in order to understand the crystallization mechanism at higher supercooling degrees.

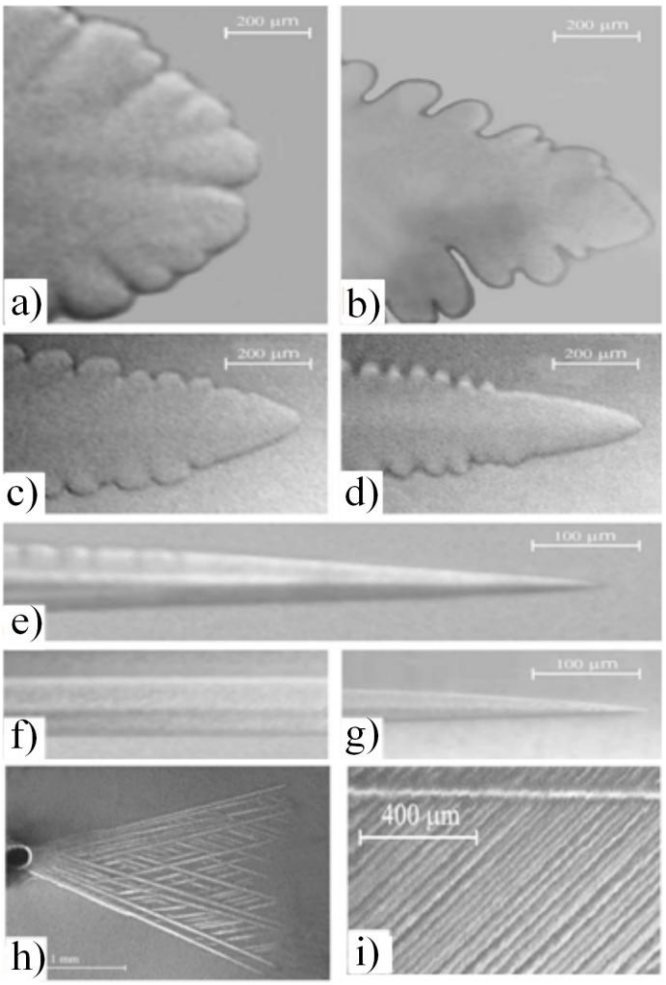

Figure 1: Various shapes of freely growing ice crystals at different initial supercooling degree for the liquid phase: Dendrite with splitted tip a) ΔT = 0.3 K; Dendrite with side-branching b) ΔT = 0.5 K, c) ΔT = 0.7 K, d) ΔT = 1.1 K, e) ΔT = 3.8 K; Branchless dendrite (needle-like crystal) f) and g) 4.2 K; Array of needles h) 8.2 K, i) 14.5 K. (Shibkov et al. 2003)

Nomenclature

c	specific heat capacity (J/kgK)
k	heat conductivity (W/mK)
k_{kin}	kinetic coefficient
L	latent heat of crystallization (J/kg)

$\vec{n}$ unit vector normal to solid-liquid interface (m)
Pe Peclét number
T temperature (K)
T_m melting/crystallization temperature (K)
$\vec{v}$ solid-liquid interface velocity (m/s)

Greek letters

Γ capillary constant (mK)
Ξ solid-liquid interface
Δ dimensionl. supercooling
ΔT supercooling/undercooling (K)
Φ level set distance function (m)
Ω phase of the domain
α thermal diffusivity (m^2/s)
δ_c capillary length (m)
δ_d diffusion length (m)
κ curvature of solid-liquid interface (1/m)
ρ density (kg/m^3)
σ interfacial tension (kg/s^2)

Subscripts

I solid-liquid interface
l liquid
n normal to the solid-liquid interface
s solid
t tip of needle-like dendrite
v volumetric property

II. Theoretical Background

Mathematically, the problem of crystallization is considered as a two-phase moving boundary case (Alexiades & Solomon 1993, Davis 2001). Both the liquid and the solid phases are active, i.e. the heat conservation is solved in both sub-domains. Heat flows from the interface in both directions. We consider a domain D of pure water where the water is either in liquid (supercooled) or solid phase. Let $T(\vec{x},t)$ represent the temperature of the water. The region where the water is in solid state is denoted as Ω_s and the region where the water is liquid as Ω_l.

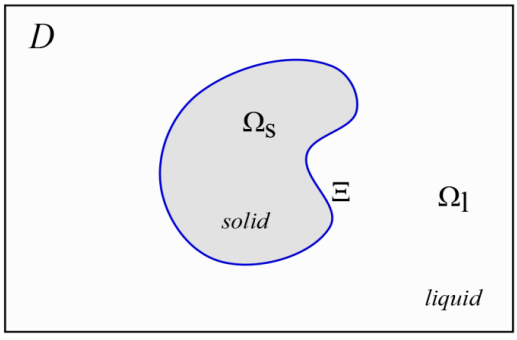

Figure 2: Schematic of the domain considered

The interface between the solid and the liquid phases is of infinitesimal thickness and is denoted as Ξ (Figure 2). As the motion in liquid region is not presently considered, the energy equation describing time dependent heat conduction in both regions reduces correspondingly to:

$$\int_V \frac{\delta(\rho c_{v,s} T)}{\delta t} dV = \oint_S (k_s \nabla T)\cdot \vec{n} dS\,, \qquad \vec{x}\in\Omega_s\,, \quad (1)$$

$$\int_V \frac{\delta(\rho c_{v,l} T)}{\delta t} dV = \oint_S (k_l \nabla T)\cdot \vec{n} dS\,, \qquad \vec{x}\in\Omega_l\,. \quad (2)$$

At the interface two boundary conditions (BC) are needed to close the computational model. Here, $\rho := \rho_s = \rho_l$ is assumed. The first one (1st BC) describes the energy balance (Stefan condition). It expresses the dependence of the local normal velocity of the interface on the heat flux discontinuity at the interface

$$\rho L \vec{v}_n = -k_l \frac{\partial T}{\partial \vec{n}}\bigg|_{\Xi,l} + k_s \frac{\partial T}{\partial \vec{n}}\bigg|_{\Xi,s}\,, \qquad \vec{x}\in\Xi\,. \quad (3)$$

This boundary condition is valid only for a flat freezing interface. The second boundary condition (2nd BC) at the interface relates to the temperature distribution. In the case of a curved interface the temperature at the interface needs to be described by the Gibbs-Thomson relation:

$$T_I = T_m - \Delta T_v = T_m\left(1 - \frac{\sigma}{\rho L}\kappa\right) = T_m - \Gamma\kappa\,, \quad (4)$$

here ΔT_v represents the capillary undercooling.
For a curved interface the correct Stefan condition (1st BC) reads:

$$\rho\left(L - \Delta c_v\left[T_m - T_I\right]\right)\vec{v}_n = -k_l \frac{\partial T}{\partial \vec{n}}\bigg|_{\Xi,l} + k_s \frac{\partial T}{\partial \vec{n}}\bigg|_{\Xi,s}\,, \quad (5)$$

where $\Delta c_v := c_{v,l} - c_{v,s} = \text{const.}$

Kinetic effects

The solid-liquid interface is in a dynamic equilibrium when the molecules attach and detach continually at equal rates. In this case, the temperature of the interface, T_I, is equal to T_m. In the case of a curved solid-liquid interface, the interface temperature is appropriately altered in order to account the capillary undercooling, Eq. (4). For the case that $T_I < T_m$, molecules become more strongly bounded to the interface. Thus, their number detaching per unit time decreases. The interface velocity, $\vec{v}_n$, increases according to the difference between T_m and T_I. Until the point where the molecules in the liquid become sluggish and the rate of attachment decreases. Hence, for pure substances with low latent heats, like metals, the velocity of the solid-liquid interface is approximated as a linear function of the kinetic undercooling, ΔT_{kin} :

$$\vec{v}_n = k_{kin}(T_m - T_I) = k_{kin}\ \Delta T_{kin}\,. \tag{6}$$

with k_{kin} representing the kinetic coefficient. Thus, the effect of the kinetic undercooling at the interface can be modelled as follows:

$$T_I = T_m - k_{kin}^{-1}\ \vec{v}_n\,. \tag{7}$$

The latent heat of metals is comparable to that of water (Table 1); accordingly this approximation should also be valid for water. Hence, in accordance with literature, the interface velocity can be approximated as a linear function of the initial supercooling (e.g. Davis 2001).

Pure substance	Latent heat, L[kJ/K]
Aluminium	398
Magnesium	368
Nickel	197
Water	333

Table 1: Latent heat of crystallization; metals vs. water.

From planar freezing interface to the growth of needle-like dendrites

The solid-liquid interface, which represents the phase-transition region where solid and liquid coexist, appears planar for most pure materials under ordinary freezing conditions (at a constant T_m), Figure 3 I. During the chrystallization of supercooled water the interface between the solid and the liquid phase becomes unstable and its microstructure appears to be dendritic. The supercooling intensity represents the destabilizing effect of the interface and the rate of solidification depends upon the degree of solidification that drives it. On the contrary, the interfacial tension tends to stabilize the interface bringing small perturbations back in line; the process described by the Gibbs-Thomson relation (Figure 3 II.) acts towards the interface stabilization. The balance between these two effects can be analyzed by the classical approach to morphological instability introduced by Mullins & Sekerka (1963a, 1963b) in the context of directional solidification (Figure 3 III.). The concept of this approach is basically exhibited in the simple setting of a two-dimensional steady-state directional solidification (Davis 2001). By utilizing this approach one can study the stability of a flat-interface solution under small sinusoidal perturbations. Two heaters are placed at the same distance, Δy, from the interface, the lower one has a constant temperature $T_s < T_m$ and the upper one is held at a constant temperature $T_l > T_m$. The analysis of the morphological instability yields the cutoff wavelength, which represents the largest possible wavelength for a stable interface:

$$\lambda_c = 2\pi\sqrt{\frac{2\alpha}{\vec{v}_{n,0}}\frac{T_m \sigma c_v}{L_v^2}} = 2\pi\sqrt{\delta_d \delta_c}\,, \tag{8}$$

where $k_s = k_l = k$, $c_s = c_l = c$, $\rho_s = \rho_l = \rho$, $\vec{v}_{n,0}$ is the constant speed of the setup along the y-axis, while the interface remains flat and stationary at $y = 0$. In other words, $\vec{v}_{n,0}$ represents the velocity of the non-perturbed interface given that the temperature gradient at the lower and upper boundary of the setup held at constant value. Assuming that the thermal diffusivity, α, and the heat capacity, c_v, are constant, the cutoff wavelength depends directly on $\vec{v}_{n,0}$. If the value of the interface velocity increases, the largest possible wavelength for a stable interface decreases. The cutoff wavelength gets smaller at higher supercooling for the liquid phase subject to the condition complying with the constant temperature gradient in the solid. In Figure 1 various shapes of freely growing ice crystals at different initial supercooling for the liquid phase are shown. In these experiments it has been observed that when a trigger (a needle in Shibkov's experiments) reaches the surface of the supercooled pure water film an ice crystal freely grows from the point of contact. The corresponding temperature jump is caused by the release of the latent heat of crystallization.

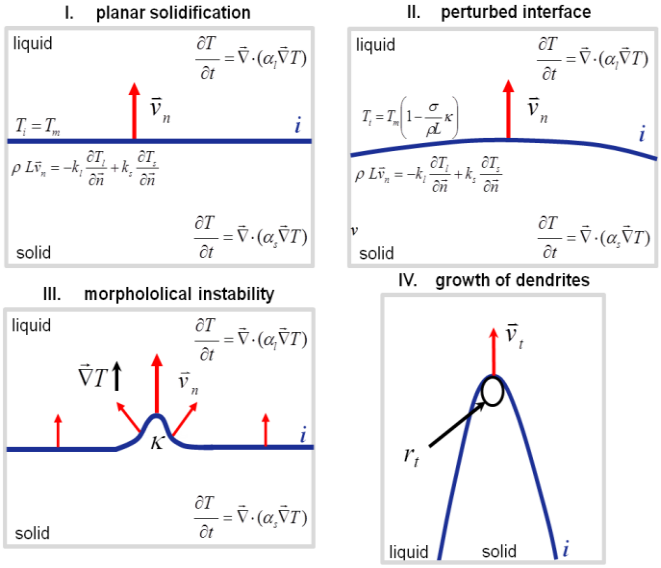

Figure 3: Sequence of events, from planar freezing front towards the growth of needle-like dendrites

Regardless of the level of the initial supercooling degree in the water, the incipient structure of the crystal is a smooth circular disk at constant value of temperature, T_m. In a second step, the disk develops some bulges which grow into fingers. These bulges, caused by a fluctuating thermal noise at the smooth interface, are exposed to a steeper temperature gradient and hence evolve into the deformation of fingers. During this transition process the primary fingers develop into crystals of different shapes: from dendrites with side-branching to needles. This transition depends strongly on the initial supercooling degree of the pure water. The critical nucleation radius is defined as

$$R_c = \frac{2\sigma\ T_m}{L_v\ \Delta T}\,. \tag{9}$$

Only when the radius of the initial nucleus is larger than R_c, it will grow to $R = \infty$. The nucleus grows as a smooth spherical sphere as far as the critical radius of instability, R_I, is achieved. When the nucleus radius is larger than R_I, the destabilizing effect (supercooling) starts to destabilize the system: small bumps (instabilities) on the interface start to grow into the supercooled water (Figure 4). The instability mechanism depends on the thermal boundary layer on the liquid side of the particle. Conduction in the solid would stabilize the particle, it means that it grows to larger radius before it becomes unstable. In Shibkov's experiments the temperature is constant in the nucleus and hence conduction in the solid is negligible. A bump on the interface propagates deeper into the liquid, increasing the magnitude of the temperature gradient on the liquid side. Hence, the energy balance (Stefan condition) causes a faster bump growth

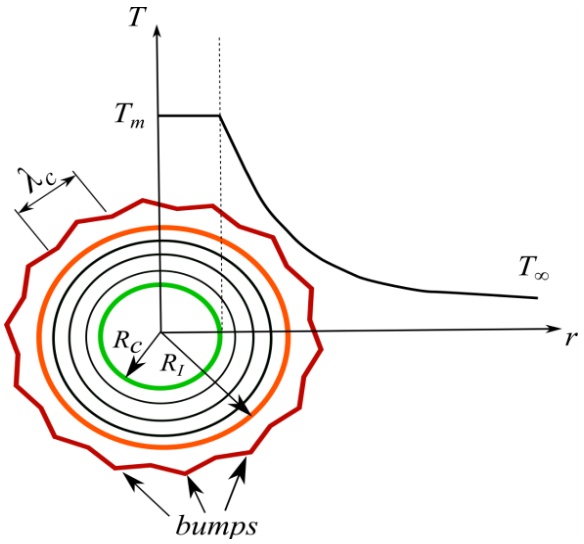

Figure 4: A sketch of a cross section of a growing spherical nucleus. Between critical nucleation radius, R_c, and critical radius of instability, R_I, the interfacial energy resists growth of bumps (smooth circular disk). Corresponding temperature profile of the initial nucleus is shown. When the nucleus radius is larger than R_I, the destabilizing effect (supercooling) starts to dominate the system: small bumps on the interface start to grow into the supercooled water.

The spacing between bumps (Figure 4) on the solid-liquid interface results from the morphological instability of Mullins & Sekerka: it is in agreement with the critical cutoff wavelength, Eq. (8), and hence it depends directly on the initial supercooling degree of the water. Small perturbations at the interface evolve into the formation of various polycrystal structures, depending on the supercooling degree. Assuming that the various crystals have a paraboloidal structure, Invantsov (1947) derived an analytical solution for the steady-state tip velocity and tip radius, under the assumption that, firstly, the kinetics is instantaneous, $k_{kin}^{-1} = 0$, and secondly, the surface tension is zero, $\sigma = 0$. This theory considers a single needle growing into an infinite half-space of supercooled liquid. The Péclet number, *Pe*, derived from the Ivantsov's theory is used to establish a correlation between the tip velocity, $\vec{v}_t$, and the tip radius, r_t:

$$Pe = \frac{r_t v_t}{2\alpha}. \qquad (10)$$

There is a unique Péclet number for the entire range of dimensionless supercooling, Δ, obtained by solving the Ivantsov function:

$$\Delta = Pe_0 \exp^{Pe_0} E_1(Pe_0). \qquad (11)$$

The solution of this function represents a continuum family of parabolas/paraboloids for a given initial dimensionless supercooling Δ. One of the first important hypothetical principle of tip selection was the marginal stability theory (MST) introduced by Langer & Müller-Krumbhaar (1977, 1978a, 1978b, 1978c) in their "Universal Law of Crystal Growth". They analyzed the stable steady-state of the Ivantsov paraboloidal dendrite, introduced the interfacial tension effect as a linearized perturbation function and found that Ivantsov's continuum family of solutions may now be divided into a stable and an unstable region. When interfacial energy, σ, is present and kinetic supercooling is neglected, a new dimensionless parameter is defined, representing the so-called "control parameter" for the "operating point" of the needle:

$$\varepsilon = \frac{T_m \sigma c_v}{L_v^2} \cdot \frac{2\alpha}{v_n} \cdot \frac{1}{r_t^2} = \frac{\delta_c \delta_d}{r_t^2} = \left(\frac{\lambda_c}{2\pi r_t} \right)^2, \qquad (12)$$

The selected dendrite corresponds to the point of marginal stability and hence the emerging tip radius, r_t, corresponds to the cutoff wavelength, λ_C, for the stability of a planar interface via the Mullins-Sekerka criterion, Eq. (8). Thus, the control parameter is evaluated as:

$$\varepsilon^* = \frac{1}{4\pi^2} \approx 0.025. \qquad (13)$$

Eq. (12) provides an additional relation between the growth velocity and the tip radius. The first relation is provided by the Peclét number (Eq. 9). On the basis of the MST, a unique growth velocity as a single valued function of the supercooling (growth law) can be calculated.

Figure 5 shows the dimensionless growth speed of freely growing ice crystals as a function of the dimensionless supercooling. The solid line represents the diffusional MST with the controlling parameter, $\varepsilon^* = 0.025$. The experimental results of Langer et al. (1978), Ohsaka & Trinh (1998), and Shibkov et al. (2005) show a deviation from the theoretical curve at high supercoolings. Shibkov et al. give as possible reason for the deviation the kinetic effects which start to influence the system at higher supercoolings. MST assumes a local thermal equilibrium at growing solid-liquid interface which may not be the case at higher supercooling degrees

because of the slow water molecular transfer across the interface (sluggish interface kinetics). Therefore, they propose that for higher supercooling degrees, the speed of solidification is predominantly determined by the mechanism of molecular attachment kinetics at the solid–liquid interface.

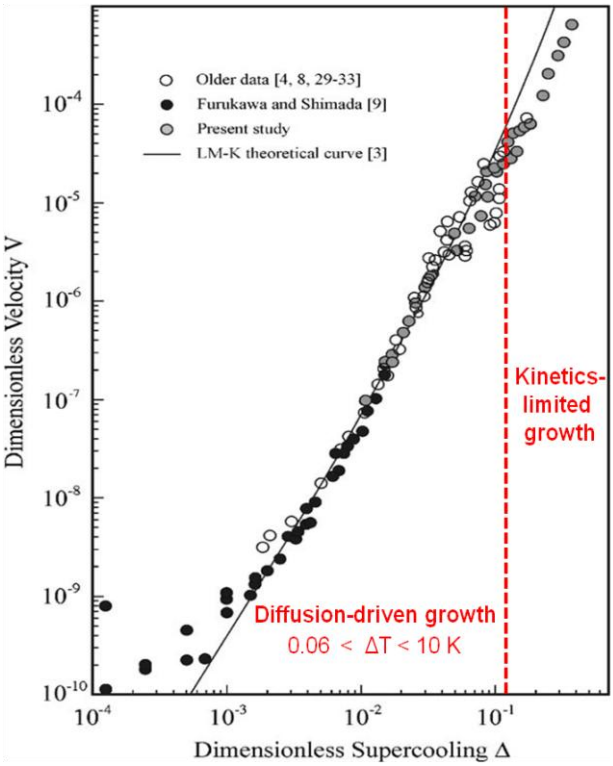

Figure 5: Ice crystals freely growing from supercooled pure water, dimensionless growth, $V = \bar{v}_t d_0 / 2\alpha$, plotted against the dimensionless supercooling, $\Delta = \Delta T\, c_p / L$ (Shibkov et al. 2005).

III. Numerical Algorithm

A computational model based on the level set method is used in this study. For a detailed description of the computational model we refer to Criscione et al. (2012). In the following, a brief introduction is given. The level set function, Φ, is defined as a signed distance function: the zero level set function represents the solid-liquid interface, whereas the signed value of the outer level set field constitutes the distance to the interface. The sign indicates the side of the interface one looks to: a negative sign of the outer level set field represents the solid phase while the positive sign indicated the liquid phase.

The heat transfer equations are solved in both, the liquid and solid phase independently from each other. At the solid-liquid interface a constant value (Dirichlet boundary condition) for the temperature field is imposed. The interface temperature is calculated according to the Gibbs-Thomson relation, Eq. (4). Here, the curvature of the solid-liquid interface (zero level set function) is needed. In cells close to the interface, the curvature is calculated in the center node as the divergence of the unit vector, $\vec{n}_\Xi = \nabla\Phi / |\nabla\Phi|$. Subtracting the normal distance between the cell center and the interface (outer level set value) from the curvature radius, one obtains the interface curvature radius. The inverse of the interface curvature radius describes the curvature of the solid-liquid interface. The temperature distribution at the solid-liquid interface of a growing crystal with four-fold anisotropy of the surface energy is illustrated in Figure 6: the interface temperature decreases at sections with positive curvature (finger tip), whereas by negative curvature (a grooving between fingers) the temperature is slightly higher than the crystallization temperature.

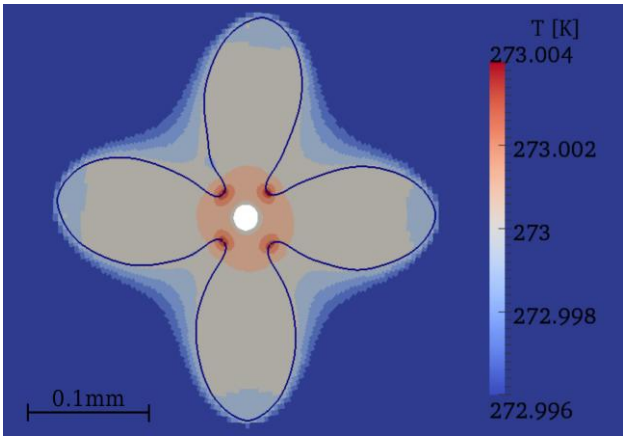

Figure 6: Gibbs-Thomson relation, temperature distribution at the interface of a growing crystal into the supercooled liquid phase; four-fold anisotropy of the interfacial tension is modelled here.

Ghost-faces and corresponding ghost points are applied to ensure accurate calculation of the temperature normal derivative at grid nodes close to the interface. This is necessary to fulfill the second boundary condition (heat flux balance), Eq. (5), at the interface. The interface temperature is stored at ghost-points. The temperature at the ghost-faces is calculated interpolating or extrapolating linearly the temperature values stored at the cell center node and the ghost-point. This value of the temperature stored at the ghost-faces is needed to approximate numerically the gradient of the temperature in the center node. Hence, the temperature in a virtual point, located at a distance normal to the interface corresponding to the half of a cell, is approximated (Taylor). Using the value of the temperature in the virtual point and the calculated interface temperature at the ghost point the normal derivative can be calculated accurately. Within a narrow band around the interface, whose width is temporally adjusted to the maximum curvature of the interface, the normal-to-interface velocity is appropriately expanded. This velocity is used to update the level set function within the narrow-band. After the update of the level set function within the band, the outer level set function is reinitialized to enable the setting a new band

around the interface in the next time step. The physical model and numerical algorithm are validated along with the analytical solution of the two-phase planar solidification.

IV. Results

Growth of an isolated needle-like dendrite including kinetic effects

The computational results of dendritic growth in Criscione et al. (2012) exhibit excellent qualitative and quantitative agreement with the Marginal Stability Theory of Langer and Müller-Krumbhaar as well as with the available experiments in the heat-diffusion growth region. At high supercooling degrees, kinetic effects start to influence the system (kinetics-limited growth). Keeping in mind that the computations (such as MST) do not account for kinetic effects, one may observe a certain deviation of the experiments from simulations at higher supercoolings. Shibkov et al. (2005) found also a substantial disagreement between experimental results and predictions of the diffusional law of dendritic growth at high supercooling degrees (Figure 5). They concluded that the observed disagreement is caused by the crossover from the diffusion-driven growth regime to the kinetics-limited regime of solidification. The kinetics growth is determined by the rate of molecular rearrangements at the interface from the liquid to solid state.

In the literature, the velocity of the solid-liquid interface at a high supercooling degree is approximated by a linear function of the kinetic undercooling, ΔT_k, Eq. (6). This approximation should be valid for pure substances with low latent heat of crystallization such as metals and water (see Table 1). To date, the definition of the kinetic coefficient, k_{kin}, is not well understood. In the following, a derivation for the kinetic coefficient is given. First of all, we assume that the steady-state dendrite velocity from experimental data (Shibkov et al. 2005), $\vec{v}_{n,\exp}$, is directly proportional to

$$\vec{v}_{n,\exp} \sim \Delta T_T \,. \tag{14}$$

ΔT_T represents the total undercooling at the solid-liquid interface, which is defined as

$$\Delta T_T = \Delta T_v + \Delta T_{kin} \,, \tag{15}$$

At a high undercooling degree the steady-state velocity obtained theoretically (MST) deviates significantly from the experimental data. Here the effect of kinetic undercooling is of decisive importance. For instance, in the case of an initial supercooling value of 15 K, MST predicts a steady-state interfacial velocity of 15,88 cm/s. The steady-state dendrite velocity originating from experiments of Shibkov amounts approximately 4 cm/s. In MST the viscous force at the solid-liquid interface is taken into account and hence the viscous undercooling. In order to account for the kinetic undercooling, the ratio of the theoretical steady-state velocity (MST) to the experimental value, $\left|\Delta\vec{v}_n\right|$, is computed and we assume that

$$\Delta T_T \cong \frac{\Delta T_v}{\left|\Delta\vec{v}_n\right|} \,. \tag{16}$$

Inserting it into Eq. (15) and assuming a linear function for the kinetic undercooling, Eq. (6), we obtain for the kinetic coefficient

$$k_{kin} \cong \frac{\left|\Delta\vec{v}_n\right| \; \vec{v}_{n,MST} \; L\rho}{\left(1-\left|\Delta\vec{v}_n\right|\right) \; \kappa\sigma \; T_m} \,. \tag{17}$$

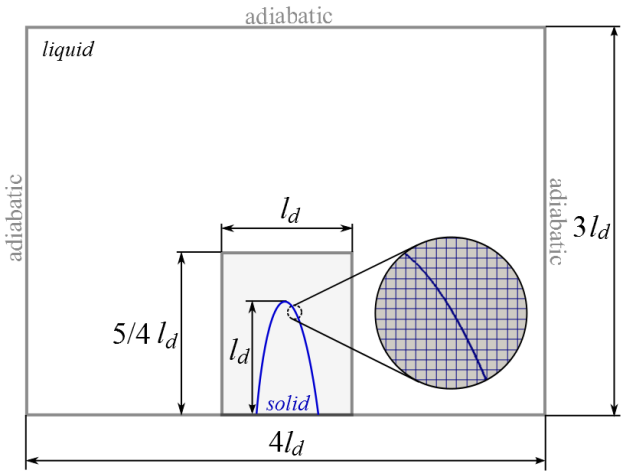

Figure 7: Schematic of the computational domain and mesh detail in the fine resolution region.

Thus, preliminary results obtained at high supercooling degrees after accounting for the kinetic undercooling in our computational model – by applying new definition of the kinetic coefficient, Eq. (17) - exhibit good agreement with the experimental data. The limitation by using Eq. (17) is that the kinetic coefficient is directly dependent on the theoretical steady-state velocity and hence on the initial supercooling degree. In order to find a universal constant being valid for all supercoolings, the relation between the kinetic coefficient and the steady-state velocity from theoretical data is approximated by following relation:

$$k_{kin}^{\,*} = \frac{1}{2}\left(\frac{2\pi}{11}\vec{v}_{n,MST}\right)^{2/3} \,. \tag{18}$$

Assuming that the solid-liquid interface approximates the theoretical value $\vec{v}_{n,MST}$ neglecting the kinetic effects, the kinetic undercooling is defined as follows:

$$\Delta T_{kin} = \frac{\left(\bar{v}_n\right)^{1/3}}{k_{kin}^{*}} . \qquad (19)$$

A schematic of the appropriate computational domain is depicted in Figure 7. The parabolic needle-like dendrite is initialized in the fine-resolution region. In order to assure a correct curvature reproduction, the curvature radius of the tip is resolved with approximately twenty grid cells. The grid resolution in this region is adjusted to the decreasing curvature radius at higher supercooling degrees. l_d represents the initial height of the parabolic needle. Other geometric parameters of the computational domain have to be selected in accordance with the vertical and horizontal growth of the needle, which directly depend on the supercooling degree. In order to fulfill the infinity conditions, adiabatic boundary conditions for the temperature solution have to be prescribed at the left, right and upper domain boundary.

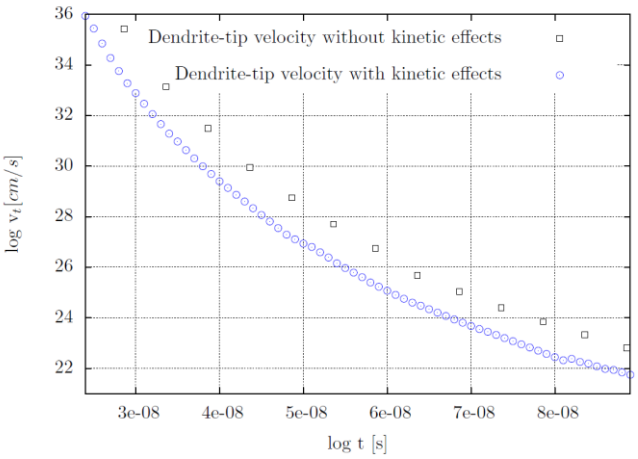

Figure 8: Tip velocity with and without kinetic effects as a function of time at a supercooling of ΔT = 10 K.

In Figure 8 the tip velocity of the parabolic needle-dendrite is plotted against the time in a specific time range. It is shown how the dendritic velocity decreases including kinetic effects at the solid-liquid interface. The kinetic undercooling (Eq. 20) influences the temperature at the solid-liquid interface and hence the heat flux released into the liquid phase decreases at increasing interface velocity. Figure 9 displays the results from our computational model compared to the theoretical and experimental data. The numerical results obtained by neglecting the kinetic undercooling exhibit excellent agreement with the diffusional Marginal Stability Theory (Criscione et al. 2012). At higher supercooling degrees, the experimental results deviate from the theoretical findings and, accordingly, to our afore-mentioned computational results. However, after accounting for the kinetic effects, by considering the new approach presented in this article, the computational results at high supercooling degrees follow closely the experimental results.

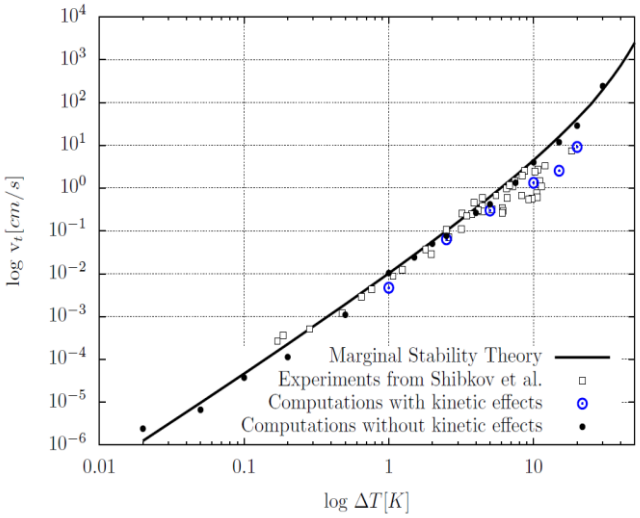

Figure 9: Numerical results vs. MST and experiments – inclusion of the kinetic undercooling at the solid-liquid interface led to improved agreement with the reference experimental

Array of needles

In typical applications at high supercooling degrees the needle crystals arrangement do not resemble an infinite collective but an array. Figure 1 illustrates an array of needles at higher supercooling degrees. From the isolated dendritic shape (with and without side-branching) at a low supercooling degree, the crystal shape evolves into the formation of needle arrays due to high destabilizing factor. The formation of an array implies the steady-state tip velocity of an isolated needle being not valid anymore, because the thermal boundary layer around the needle-tip is now influenced by the surrounding growing needles. Hence, to investigate numerically an array of needles, the computational setup exhibited in Figure 7 should be slightly modified, introducing symmetry conditions at the left and right domain boundary (Figure 10). A channel-like subdomain with the width, λ, is considered. The sidewalls of this channel are assumed to be perfectly insulated. Subsequently the width, λ, represents the spacing between the needles, whereas w describes the initial width of the parabolic needle-like dendrite.

Preliminary results at an initial supercooling of 15 K, neglecting kinetic undercooling, show that if λ approximates the so-called fastest growing mode the steady-state velocity of the solid-liquid interface approaches to *15.8* cm/s, which corresponds to the steady-state velocity of an isolated dendrite. Decreasing of λ reduces the steady-state velocity of the dendrite-tip till to stable growth. Whereas increasing of λ reduces the steady-state velocity of the dendrite-tip as well by unstable regime of growth.

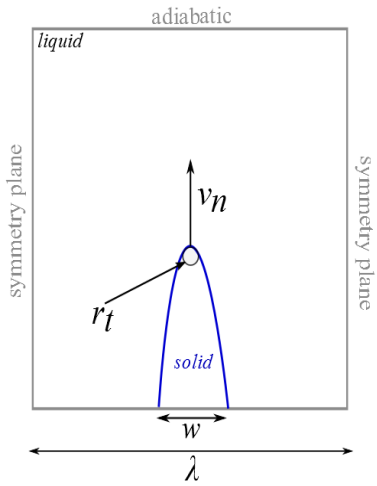

Figure 10: Schematic of two-dimensional needle-like dendrite with initial width, *w*, growing at speed $\vec{v}_n$ in an array; λ describes the spacing between the needles.

V. Conclusions

A new computational model (Criscione et al. 2012) in conjunction with an appropriate level set formulation for the numerical capturing of the interface between the supercooled and the solidified liquid is applied. Mathematically, the phenomenon of solidification is modeled by utilizing a moving boundary problem. The algorithm is capable of computing domains of arbitrary geometrical complexity and is capable of accounting for relevant influencing factors such as capillary undercooling at the liquid-solid interface. Results of dendritic growth (Criscione et al. 2012) exhibit excellent qualitative and quantitative agreement with the Marginal Stability Theory (MST) of Langer and Müller-Krumbhaar (1978) as well as with the available experiments in the heat-diffusion-dominated region (Shibkov et al. 2005). At higher supercooling degrees an evident deviation from experimental data was observed. Possible reason for this deviation is lack of kinetic effects in the computational model. On this account, a new approach for the calculation of the kinetic undercooling term is derived and implemented into the computational model. Accordingly, the results relevant to dendritic growth exhibit a substantially improved agreement with experiments also in the so-called kinetics-limited region.
Further investigations concerning the growth of needles in an array indicate that surrounding needle-like dendrites do not influence considerably the steady-state tip velocity of an isolated needle.

Acknowledgements

We thank Mr. S. Alzamil for his support in conducting part of the simulations. The authors are grateful to the German Scientific Foundation (DFG) for their support in the framework of the SFB-TRR 75 collaborative research center.

References

Alexiades, V. & Solomon, A. D. Mathematical modeling of melting and freezing Processes. Hemisphere Publishing Corporation. (1993)

Criscione, A., Kintea, D., Tukovic´, Z., Jakirlic´, S., Roisman, I.V., Tropea, C. On Computational Investigation of the Supercooled Stefan Problem. Proceedings of the 12th International Conference on Liquid Atomization and Spray Systems, Heidelberg, Germany. (2012)

Davis, S. H. Theory of Solidification. Cambridge University Press. (2001)

Do-Quang, M., Amberg, G. Simulation of free dendritic crystal growth in a gravity environment. Journal of computational physics, 227, 1772-1789. (2008)

Furukawa, Y. & Shimada, W. Three-dimensional pattern formation during growth of ice dendrites - its relation to universal law of dendritic growth . Journal of Crystal Growth, 128, 234-239. (1993)

Ivantsov, G.P. Temperature field around spherical, cylindrical, and needle-shaped crystals which grow in supercooled melt. Dokl. Akad. Nauk SSSR, 558, 567-569. (1947)

Jung, S., Tiwari, M. K., Doan, N. V., Poulikakos, D. Mechanism of supercooled droplet freezing on surfaces. Nature Communications (2012) 3:615 doi: 10.1038/ncomms1630.

Kobayashi, R.. Modeling and numerical simulations of dendritic crystal growth. Physica D: Nonlinear Phenomena, 63(3-4), 410-423. (1993)

Langer, J. S. & Müller-Krumbhaar, R. F. Stability effects in dendritic crystal growth. Journal of Crystal Growth, 42, 11-14. (1977)

Langer, J. S. & Müller-Krumbhaar, R. F. Theory of dendritic growth-I. Elements of a stability analysis. Acta Metallurgica, 26, 1681-1687. (1978a)

Langer, J. S. & Müller-Krumbhaar, R. F. Theory of dendritic growth-II. Instabilities in the limit of vanishing surface tension. Acta Metallurgica, 26, 1689-1695. (1978b)

Langer, J. S., Müller-Krumbhaar, R. F. Theory of dendritic growth-III. Effects of surface tension. Acta Metallurgica, 26, 1697-1708. (1978c) *

Langer, J.S., Sekerka, R.F., Fujioka, T. Evidence for a universal law of dendritic growth rates. J. Crystal Growth 44 (1978) 414.

Mullins, W. W. & Sekerka, R. F. Morphological stability of a particle growing by diffusion or heat flow. Journal of Applied Physics, 34, 323-329. (1963a)

Mullins, W. W. & Sekerka, R. F. The stability of a planar interface during solidification of a dilute binary alloy. Journal of Applied Physics, 35, 444-451. (1963b)

Ohsaka, K., Trinh, E.H. Apparatus for measuring the growth velocity of dendritic ice in undercooled water. J. Crystal Growth 194 (1998) 138.

Osher, S. & Sethian, J. A. Fronts propagating with curvature-dependent speed: Algorithms based on Hamilton-Jacobi formulations. Journal of Computational Physics, 79, 12-49. (1988)

Shibkov, A. A., Golovin, Yu. I., Zheltov M. A., Korolev, A. A., Vlasov A. A. Kinetics and morphology of nonequilibrium growth of ice in supercooled water. Crystallography Reports, 46, 3, 496-502. (2001)

Shibkov, A. A., Golovin, Yu. I., Zheltov M. A., Korolev, A. A., Leonov, A. A. Morphology diagram of nonequilibrium patterns of ice crystals growing in supercooled water. Physica A, 319, 65-79. (2003)

Shibkov, A. A., Zheltov M. A., Korolev, A. A., Kazakov, A. A, Leonov, A. A. Crossover from diffusion-limited to kinetics-limited growth of ice crystals. Journal of Crystal Growth, 285, 215-227. (2005)

Wheeler, A. A., Murray, B. T., Schaefer, R.J. Computation of dendrites using a phase field model. Physica D, 66, 243-262. (1993)